

The Vela pulsar and its likely counter-jet in the K_s band

D. Zyuzin, Yu. Shibano¹ and A. Danilenko

Ioffe Physical Technical Institute, Politeknicheskaya 26, St. Petersburg, 194021, Russia

R. E. Mennickent

Department of Astronomy, Universidad de Concepcion, Casilla 160-C, Concepcion, Chile

and

S. Zharikov

Observatorio Astronómico Nacional SPM, Instituto de Astronomía, UNAM, Ensenada, BC, Mexico

ABSTRACT

We report the first high spatial resolution near-infrared imaging of the Vela pulsar in the K_s band obtained with the new adaptive optics system recently mounted on the Gemini-South telescope. For the first time, we have firmly detected the pulsar in this band with $K_s \approx 21^m8$, and have resolved in detail an extended feature barely detected previously in the immediate vicinity of the pulsar in the J_sH bands. The pulsar K_s flux is fully consistent with the extension of the flat optical spectrum of the pulsar towards the infrared and does not confirm the strong infrared flux excess in the pulsar emission suggested earlier by the low spatial resolution data. The extended feature is about two times brighter than the pulsar and is likely associated with its X-ray counter-jet. It extends $\sim 2''$ southwards of the pulsar along the X-ray counter-jet and shows knot-like structures and a red spectrum.

Subject headings: infrared: stars — stars: neutron — pulsars: individual (the Vela pulsar)

1. Introduction

After the young Crab and B0540–69 pulsars with the visual magnitudes of 16^m5 and 22^m6 the 11 kyr old Vela pulsar with the magnitude of 23^m6 is the third brightest in the optical among all isolated neutron stars (NSs) known. The relative brightness has allowed to perform detailed optical studies including the successful timing, spectral, and polarization observations. Similar to the Crab pulsar, Vela has an almost flat spectrum from the near infrared (IR) to the ultra violet (UV) (Mignani et al. 2007). The similarity has been unexpectedly broken by recent *Spitzer* observations in the mid-IR, where the Vela pulsar has shown a strong flux excess over its optical-UV spectrum ex-

tension towards IR (Danilenko et al. 2011). This is completely different from Crab whose mid-IR and optical-UV spectra are described by a single power law (Sandberg & Sollerman 2009). Similar excesses have been detected only for two magnetars 4U 0142+61 and 1E 2259+586 (Wang et al. 2006; Kaplan et al. 2009), where they were interpreted as an emission from hypothetical fall-back X-ray irradiated discs around those NSs. However, Vela is not a magnetar. It is an ordinary rotation powered pulsar emitting from radio to gamma-rays and powering, like Crab, a bright (in X-rays) torus-like pulsar wind nebula (PWN) with polar jets (Helfand et al. 2001). The fall-back disk survival around such an active pulsar with a strong relativistic particle wind appears to be problematic (see, e.g., Jones 2007). Two other possibilities have been suggested to explain

¹St. Petersburg State Polytechnical Univ., Politeknicheskaya 29, St. Petersburg, 195251, Russia

the excess (Danilenko et al. 2011): a complicated distribution function of emitting particles in the NS magnetosphere; a possible contamination of the pulsar flux by an unresolved PWN structure. The first one looks very unusual, while the second is supported by the presence of a faint nebulosity $2''$ away from the pulsar tentatively detected in the near-IR VLT/ISAAC J_s and H images (Shibanov et al. 2003). The images had a higher spatial resolution than the *Spitzer* ones. It is projected onto the origin of the pulsar X-ray counterjet and has a red colour, which could, in principle, explain the mid-IR excess (Danilenko et al. 2011). To check that, one needs a higher spatial resolution imaging in the near-IR.

The Vela pulsar has never been observed in the K band. Motivated by this and by the excess problem, we have carried out a high spatial resolution imaging of the Vela field in the K_s band with the new generation of the adaptive optics (AO) system recently mounted on the Gemini-South telescope (Carrasco et al. 2012). The observations and data reduction are described in Sect. 2, the results are presented in Sect. 3 and discussed in Sect. 4.

2. Gemini-South data

2.1. Observations, data reduction, and calibration

The Vela pulsar was observed on January 30, 2013 in the K_s band with the Gemini Multi-Conjugate Adaptive Optics System (GeMS) and its near-infrared imager, the Gemini South Adaptive Optics Imager (GSAOI), mounted on the Gemini-South telescope¹. The observations were carried out in the service mode during the GeMS + GSAOI System Verification science program. The GSAOI science array is a 2×2 mosaic of four Rockwell HAWAII-2RG detectors forming a 4080×4080 pixel focal plane with a field of view of $85'' \times 85''$ and a pixel scale of $0''.02$. Each detector also contains a programmable On-Detector Guide Window (ODGW) which can provide a tip-tilt information for a combination of up to four natural guide stars in GeMS. Three natural optical guide stars, NOMAD 0448-0138807 ($R \sim 15^m6$), 0448-

0138766 (14^m2), and 0448-0138794 (14^m3) were used for the CANOPUS tip-tilt wave front sensor (CWFS), which is the AO bench of GeMS. The latter star was also the ODGW infrared guide star. The pulsar was exposed on chip 1 of the GSAOI array and we focus below on the data obtained from this chip. The observing conditions were photometric with seeing $\lesssim 0''.55$.

We have obtained 19 dithered 100 s science exposures with $\sim 10''$ offsets at an airmass of ~ 1.04 . Gemini GeMS + GSAOI twilight flat-fields were taken and used to create a master flat-field frame. Data reduction, linearity correction, sky subtraction, flat-fielding and bad pixel correction were performed using the IRAF `gemini.gsaoi` tool. The effective mean seeing, defined as the full width at half maximum (FWHM) of a stellar profile, on the chip 1 AO corrected frames was in the range of $0''.07$ – $0''.09$, depending on the individual exposure and a source position on the frame. The best seeing concentrated within $\sim 0''.3$ region around the pulsar, in accordance with expectations for our AO observational setup. Differences of instrumental magnitudes of several field stars around the pulsar in different exposures were less than 1%. The reduced frames were aligned to a single reference frame of the best image quality and summed². The resulting effective mean seeing and integration time were $0''.085$ and 1900 s, respectively. The magnitude zero-point of $C_{K_s} = 25^m53(4)$ (instrumental fluxes in ADUs) for the chip 1 was derived based on the photometric standards (9132, 9136, 9144, 9146) from Persson et al. (1998) obtained on the same night. The atmospheric extinction of 0^m065 in K_s was taken from the GSAOI web-site.

2.2. Astrometry

We have performed the relative astrometry of the K_s -band resulting image using the VLT/ISAAC J_s -band image obtained twelve years ago by Shibanov et al. (2003) as a reference frame. Nine unsaturated isolated stars located in the pulsar vicinity were selected as the reference points, and used in the IRAF `geomap/ccmap` tools to obtain the plate solutions. Formal *rms* uncertainties of the astrometric fit were $\lesssim 0''.014$ with maximum

¹<http://www.gemini.edu/sciops/instruments/gsaoi/documents>
<http://www.gemini.edu/sciops/instruments/gems/documents>

²final image located on
<http://www.ioffe.ru/astro/NSG/obs/index.html>

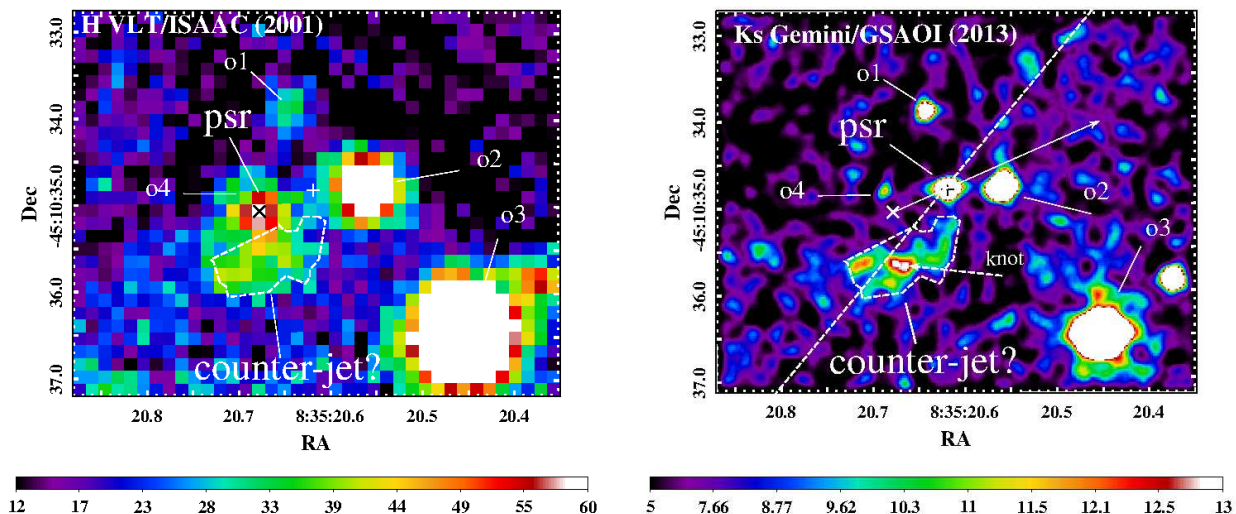


Fig. 1.— $5''.5 \times 4''.5$ fragment of the Vela pulsar vicinity as seen with the VLT/ISAAC (*left*) and Gemini/(GeMS + GSAOI) (*right*) in the H and K_s bands. The pulsar and nearby field objects are marked using notations from Shibano et al. (2003), except “o4”, which is detected only with Gemini. The K_s image is smoothed with a seven-pixel Gaussian kernel to better underline the morphology of the extended feature, presumably the counter-jet emanating from the pulsar. The long-dashed line in the right frame indicates the projection of the X-ray counter-jet axis on the sky. Symbols “ \times ” and “ $+$ ” mark the pulsar positions at the epochs of the VLT (2001) and Gemini (2013) observations, respectively. The long and short arrows indicate the direction of the pulsar proper motion and the position of a bright knot within the extended feature, respectively. The polygon is the aperture used for photometry of the feature.

residuals of $\lesssim 0''.032$ for both coordinates. Taking into account the uncertainties of the reference star positions, which were $\lesssim 8$ mas and $\lesssim 0.2$ mas for the VLT and Gemini images, respectively, a conservative 1σ referencing uncertainty of the Gemini image with respect to the VLT ones is $\lesssim 0''.02$. Adopting the VLT absolute astrometric image referencing from Shibano et al. (2003), the absolute astrometric uncertainties of the Gemini K_s -band image is $\approx 0''.21$.

3. Results

3.1. Identification of the pulsar and a likely counterpart of its counter-jet

A fragment of the resulting K_s image demonstrating the Vela pulsar vicinity is shown in the *right panel* of Fig. 1. It is compared with a similar fragment obtained in the H band with the VLT/ISAAC by Shibano et al. (2003) (*left panel*). We consider a point-like object marked by “ $+$ ” and detected in K_s at $\sim 20\sigma$ significance as the Vela pulsar counterpart candidate. In the K_s image, there is also an extended feature adjacent to the counterpart candidate from the south.

The feature is also barely resolved in the H band, which means that it is not an artifact.

The position of the suggested pulsar counterpart in the K_s image is shifted by $0''.68 \pm 0''.05$ with respect to the pulsar position at the epoch of the VLT observations (2001). The shift implies a proper motion $\mu = 56 \pm 4$ mas yr $^{-1}$ with positional angle $PA = 296^\circ.0 \pm 4^\circ.3$, which is consistent with the pulsar proper motion $\mu = 58 \pm 0.1$ mas yr $^{-1}$ and $PA = 301^\circ.0 \pm 1^\circ.8$ based on radio observations (Dodson et al. 2003). This is a strong evidence that the point-like object detected in the K_s image is the pulsar. None other point-like object in the pulsar vicinity demonstrates any significant proper motion.

The extended feature was named “counter-jet?” by Shibano et al. (2003), assuming its possible association with the counter-jet of the Vela torus-like X-ray PWN. The Gemini AO observations confirm this structure with a higher significance and reveal important details of its morphology. It extends southwards from the pulsar by about $2''$ along the X-ray counter-jet axis with $PA \approx 130^\circ$ (Helfand et al. 2001) marked by the dashed line in the *right panel* of Fig. 1. This supports

the association of the extended feature with the Vela X-ray counter-jet. In X-rays the counter-jet extends to a much larger distance up to $1'$. In the near-IR it is likely that we see only its origin near the pulsar. The K_s -band counter-jet demonstrates a non-uniform morphology with several knots. The brightest knot is in the center of the feature. It is marked in Fig. 1 and is reminiscent of the knot structure $0''.6$ away from the Crab pulsar, which is also projected onto the counter-jet origin of the Crab PWN (Hester et al. 1995). The Vela IR counter-jet is not detected in the optical range with the *HST* (Shibanov et al. 2003) whose spatial resolution is comparable to that of Gemini/GSAOI. This implies that it has a very red spectrum. Also it becomes evident, that the putative counter-jet and the pulsar cannot be resolved from each other in the significantly lower spatial resolution *Spitzer* mid-IR images analyzed by Danilenko et al. (2011).

In the Gemini image we do not find any other extended structure that could be identified with other parts of the Vela PWN. In particular, we do not see the inner arc whose marginal detection in J_s was discussed by Shibanov et al. (2003). In addition to the o1–o3 point-like objects from the pulsar neighborhood considered earlier (Shibanov et al. 2003; Danilenko et al. 2011) we find a red point-like source “o4” detected east of the pulsar at $\sim 5\sigma$ confidence only in the K_s image. It is significantly fainter than the pulsar and was partially overlapped with it at the VLT observation epoch.

3.2. Photometry

For stellar-like object photometry we used a circular aperture with four pixels radius, comparable to the effective seeing of the K_s image. The correction for finite aperture, derived from the point spread function (PSF) of bright stars located close to the pulsar, is $\delta m = 0.64(2)$. In this case, uncertainties include the PSF variation over the selected image section. For the counter-jet we used a polygon aperture shown in Fig. 1, although the final results depend weakly on the specific aperture shape and background region parameters.

We have also remeasured the spatially integrated brightnesses of the counter-jet in the J_s and H bands. The photometry was performed on the VLT/ISAAC pulsar subtracted

images (Shibanov et al. 2003, Fig. 1). Our results differ significantly from those presented by Danilenko et al. (2011). The reason is that the authors used mean surface brightnesses from Shibanov et al. (2003) which were accidentally overestimated by $1.94 \text{ mag arcsec}^{-2}$ in both bands. After this correction the fluxes from Shibanov et al. (2003) are consistent with our ones. All measured fluxes were de-reddened using $E_{B-V} = 0.055(5)$ and $R_V = 3.1$ (Shibanov et al. 2003). The results are summarized in Table 1.

For completeness, K_s magnitudes of o1, o2, o3, o4 field objects are $22^m48(8)$, $20^m53(4)$, $18^m77(4)$, and $23^m2(2)$, respectively. The derived 3σ detection limit for a point-like object for a $0''.3$ aperture (corresponding to $\gtrsim 90\%$ of a point-like source flux) centered at some position in the pulsar vicinity free from any sources is 23^m6 .

3.3. Spectra of the Vela pulsar and its “counter-jet”

Using our photometry results, in Fig. 2 we show an upgrade of the IR-UV spectra of the pulsar and its likely counter-jet compiled recently by Danilenko et al. (2011). One sees that the K_s flux of the pulsar agrees well with the extrapolation of its flat power law UV-optical spectrum toward the longer wavelengths. This makes the Vela pulsar spectral energy distribution (SED) similar to that of the younger Crab (Sandberg & Sollerman 2009).

At the same time, the counter-jet spatially integrated K_s flux (shown by red symbol in Fig. 2) is about twice as high as the pulsar flux. The counter-jet J_sHK_s fluxes demonstrate a very steep power law SED with a spectral index of about three. The Spitzer fluxes are compatible with the long wavelength extrapolation of this SED, suggesting a common nature of the near-IR and mid-IR emission. We have checked that the essentially non-thermal, likely synchrotron, spectrum of the counter-jet is different from blackbody-like SEDs of the nearby stellar objects o1, o2, o3. This means that the extended feature can hardly be just a combination of faint blended stars.

Table 1: Magnitudes and fluxes of the pulsar and the counter-jet feature (defined by the polygon in Fig. 1) observed and dereddened with $E_{B-V} = 0.055(5)$ and $R_V = 3.1$.

λ_{eff} (band), μm	Observed		Dereddened	
	Mag. ^a	$\log F_\nu$, μJy	Mag.	$\log F_\nu$, μJy
pulsar				
1.23(J_s) ^b	22.71(10)	0.14(4)	22.66(10)	0.16(4)
1.65(H) ^b	22.04(18)	0.21(7)	22.00(18)	0.23(7)
2.16(K_s)	21.76(6)	0.12(2)	21.74(6)	0.13(2)
counter-jet				
1.23(J_s)	24.14(37)	-0.43(15)	24.09(37)	-0.41(15)
1.65(H)	22.35(10)	0.09(8)	22.31(10)	0.11(8)
2.16(K_s)	21.16(8)	0.36(3)	21.14(8)	0.37(3)
<i>Spitzer</i> data on the pulsar + counter-jet feature				
3.6 ^c	18.48(22)	1.06(9)	18.48(22)	1.06(9)
4.5 ^c	$\gtrsim 16.84$	$\lesssim 1.52$	$\gtrsim 16.84$	$\lesssim 1.52$
5.8 ^c	16.38(27)	1.51(11)	16.38(27)	1.51(11)
8.0 ^c	$\gtrsim 15.58$	$\lesssim 1.70$	$\gtrsim 15.58$	$\lesssim 1.70$

^anumbers in brackets are 1σ uncertainties referring to the last significant digits quoted

^b J - and H -band data are from Shibano et al. (2003)

^cmid-IR data are from Danilenko et al. (2011)

4. Discussion

The Gemini-South ground-based observations with the new generation of the AO system have provided us with the superb image quality comparable to that of the *HST*. This allowed us to firmly detect, for the first time, the Vela pulsar in the K_s band. The measured pulsar flux is consistent with the extrapolation of the pulsar optical-UV spectrum towards the IR, which shows that the spectrum remains flat in this range and does not demonstrate any excess suggested early by the lower spatial resolution IR data. The AO observations also enabled us to confirm and resolve the feature extended immediately behind the pulsar. The elongation of the extended feature in the direction of the X-ray counter-jet and in the opposite direction of the pulsar proper motion suggests that it can be associated with the X-ray counter-jet. This is supported by the compact and relatively bright knot-like structure within the feature (Fig. 1), which is reminiscent of the well known optical-near-IR knot within the south-east jet of

the Crab pulsar.

The likely non-thermal spectrum of the Vela IR counter-jet is also similar to the spectrum of the Crab knot, which follows the power law with a spectral index of 1 and is responsible for an apparent excess of the Crab-pulsar mid-IR fluxes observed with *Spitzer* (Sandberg & Sollerman 2009). The spectrum of the Vela counter-jet is even steeper resulting in a much stronger apparent excess of the Vela flux in the mid-IR. Our data practically rule out alternative interpretations of the mid-IR excess discussed by Danilenko et al. (2011), such as the fall-back disk or the complicated emitting particle distribution function in the pulsar magnetosphere. The Vela counter-jet spectrum is also consistent with typically red spatially integrated optical-IR spectra of PWNe (Zharikov et al. 2013).

The Crab knot (Sandberg & Sollerman 2009), and Vela jets (Pavlov et al. 2001) are known to demonstrate a high temporal variability even on a week scale. The current data do not allow one

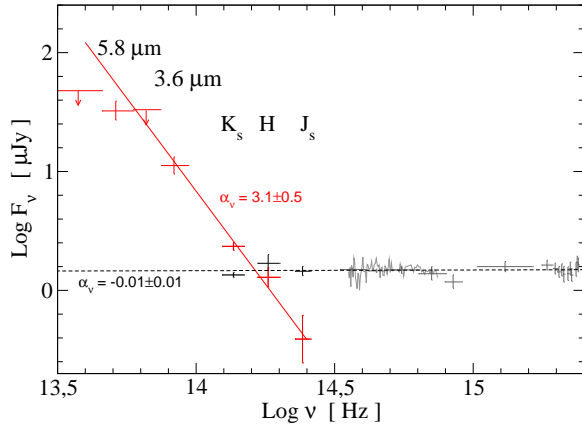


Fig. 2.— IR-UV spectra of the Vela pulsar (black) and the likely counter-jet feature (red). The UV-optical data are from Romani et al. (2005) and Mignani et al. (2007), the IR data are from Shibano et al. (2003) and Danilenko et al. (2011). The dashed line approximates the flat UV-optical spectrum of the pulsar. The red line is the best fit to the near-IR fluxes of the counter-jet. The index α_ν is defined as $F_\nu \propto \nu^{-\alpha_\nu}$.

to infer whether the Vela IR counter-jet is variable and move together with the pulsar. Detection of such variability would thus serve as a strong evidence for its PWN nature. This can also help to discard possible alternative interpretations, such as a Vela supernova remnant filament or a background galaxy at a cosmological distance. Some marginal evidence of the feature variability has been reported by Shibano et al. (2003) based on the VLT near-IR observations. Forthcoming VLT/NACO and *Spitzer* data will hopefully find out whether the detected feature is variable, clarify its spectrum and real nature. Observations at longer wavelengths are important to confirm power law spectrum of the feature. To detect other parts of the Vela PWN, deeper near-IR observations are necessary.

We are grateful to the Gemini AO system team for performing excellent observations and to the anonymous referee for useful comments. The work was partially supported by the Russian Foundation for Basic Research (grants 11-02-00253 and 13-02-12017-ofi-m), RF Presidential Program (Grant NSh 4035.2012.2), and by CONACYT

151858 project. REM acknowledges support by the BASAL Centro de Astrofísica y Tecnologías Afines (CATA) PFB-06/2007.

Facilities: Gemini.

REFERENCES

- Carrasco, E. R., Edwards, M. L., McGregor, P. J., et al. 2012, in Society of Photo-Optical Instrumentation Engineers (SPIE) Conference Series, Vol. 8447, Society of Photo-Optical Instrumentation Engineers (SPIE) Conference Series
- Danilenko, A. A., Zyuzin, D. A., Shibano, Y. A., & Zharikov, S. V. 2011, MNRAS, 415, 867
- Dodson, R., Legge, D., Reynolds, J. E., & McCulloch, P. M. 2003, ApJ, 596, 1137
- Helfand, D. J., Gotthelf, E. V., & Halpern, J. P. 2001, ApJ, 556, 380
- Hester, J. J., Scowen, P. A., Sankrit, R., et al. 1995, ApJ, 448, 240
- Jones, P. B. 2007, MNRAS, 382, 871
- Kaplan, D. L., Chakrabarty, D., Wang, Z., & Wachter, S. 2009, ApJ, 700, 149
- Mignani, R. P., Zharikov, S., & Caraveo, P. A. 2007, A&A, 473, 891
- Pavlov, G. G., Kargaltsev, O. Y., Sanwal, D., & Garmire, G. P. 2001, ApJ, 554, L189
- Persson, S. E., Murphy, D. C., Krzeminski, W., Roth, M., & Rieke, M. J. 1998, AJ, 116, 2475
- Romani, R. W., Kargaltsev, O., & Pavlov, G. G. 2005, ApJ, 627, 383
- Sandberg, A., & Sollerman, J. 2009, A&A, 504, 525
- Shibano, Y. A., Koptsevich, A. B., Sollerman, J., & Lundqvist, P. 2003, A&A, 406, 645
- Wang, Z., Chakrabarty, D., & Kaplan, D. L. 2006, Nat, 440, 772
- Zharikov, S. V., Zyuzin, D. A., Shibano, Y. A., & Mennickent, R. E. 2013, A&A, 554, A120

This 2-column preprint was prepared with the AAS L^AT_EX macros v5.2.